HHS Public Access

Author manuscript

Neuroimage. Author manuscript; available in PMC 2016 September 01.

Published in final edited form as:

Neuroimage. 2015 September ; 118: 183–192. doi:10.1016/j.neuroimage.2015.05.045.

Laminar Specific Detection of APP induced Neurodegeneration and Recovery using MEMRI in an Olfactory based Alzheimer's Disease Mouse Model

Galit Saar[a], **Ning Cheng**[b,c], **Leonardo Belluscio**[b], and **Alan P. Koretsky**[a,*]

[a]Laboratory of Functional and Molecular Imaging, National Institute of Neurological Disorders and Stroke, National Institutes of Health, Bethesda, MD 20892, USA

[b]Developmental Neuronal Plasticity Unit, National Institute of Neurological Disorders and Stroke, National Institutes of Health, Bethesda, MD 20892, USA

[c]Alberta Children's Hospital Research Institute (ACHRI), Cumming School of Medicine, University of Calgary, Calgary, AB T2N 4N1, Canada

Abstract

Manganese Enhanced MRI (MEMRI) was used to detect specific laminar changes in the olfactory bulb (OB) to follow the progression of amyloid precursor protein (APP)-induced neuronal pathology and its recovery in a reversible olfactory based Alzheimer's disease (AD) mouse model. Olfactory dysfunction is an early symptom of AD, which suggests that olfactory sensory neurons (OSNs) may be more sensitive to AD related factors than neurons in other brain areas. Previously a transgenic mouse model was established that causes degeneration of OSNs by overexpressing humanized APP (hAPP), which results in a disruption of olfactory circuitry with changes in glomerular structure. In the present work, OB volume and manganese enhancement of the glomerular layer in OB were decreased in mutant mice. Turning off APP overexpression with doxycycline produced a significant increase in manganese enhancement of the glomerular layer after only 1 week, and further recovery after 3 weeks, while treatment with Aβ antibody produced modest improvement with MRI measurements. Thus, MEMRI enables a direct tracking of laminar specific neurodegeneration through a non-invasive *in vivo* measurement. The use of MRI will enable assessment of the ability of different pharmacological reagents to block olfactory neuronal loss and can serve as a unique *in vivo* screening tool to both identify potential therapeutics and test their efficacy.

Keywords

Manganese enhanced MRI; olfaction; Alzheimer's disease; Molecular Imaging

*Corresponding author: National Institute of Neurological Disorders and Stroke, National Institutes of Health, 10 Center Drive, Bldg. 10, Rm. B1D728, MSC 1065, MD 20892, USA, koretskya@ninds.nih.gov, Phone: +1-301-402-9659..
Galit Saar: saarg@mail.nih.gov, Ning Cheng: ncheng@ucalgary.ca, Leonardo Belluscio: belluscl@mail.nih.gov

Introduction

A pathological hallmark of Alzheimer's disease (AD), one of the most common neurodegenerative diseases in the world, is the presence of extracellular plaques of amyloid-β (Aβ), which are small peptides derived from amyloid precursor protein (APP). Aβ accumulation, together with intracellular neurofibrillary tangles (NFTs) accumulation, is associated with large scale neuronal loss in late stages of AD (Hardy and Selkoe, 2002). Olfactory dysfunction is an early symptom of AD (Bacon et al., 1998) with Aβ pathology in the olfactory epithelium (OE), which correlates to brain pathology of AD patients (Talamo et al., 1989, Arnold et al., 2010). This suggests that olfactory sensory neurons (OSNs) may be more sensitive to AD related factors than other brain regions. OSNs regenerate continuously throughout life and project their axons directly to olfactory bulb (OB) glomeruli, which results in a defined neuronal circuitry (Farbman, 1990, Calof et al., 1996). Therefore, the olfactory system can serve as a model for the study of APP induced neurodegeneration and its recovery.

A reversible olfactory based mouse model of amyloid induced AD recently established that degeneration in mature OSNs can be rapidly induced by simply overexpressing a humanized APP (hAPP) (Cheng et al., 2011). In a later study it was shown that APP expression in OSNs induced circuit disruption in the OB, particularly in the glomerular layer. This OB circuit disruption could be partly restored by turning off hAPP expression (Cheng et al., 2013).

MRI has been widely used to assess AD status and its progression in humans. Hippocampal atrophy and ventricular enlargement have been consistently found in AD and mild cognitive impairment stages (MCI) (Jack et al., 2004b, Thompson et al., 2004, Ridha et al., 2008, Tang et al., 2014), enabling MRI to serve as a biomarker for AD (Dubois et al., 2010, Jack et al., 2011). Aβ plaques are a hallmark biomarker for AD that precedes the onset of dementia. However, MRI detection of these plaques directly is currently limited to animal models of AD (Wadghiri et al., 2003, Helpern et al., 2004, Jack et al., 2004a, Zhang et al., 2004). Positron emission tomography (PET) ligands that target amyloid have been used for imaging of Aβ accumulation in the brain (Klunk et al., 2004, Rowe et al., 2008, Vandenberghe et al., 2010) which, when combined with MRI studies of degeneration, enable continuous detection of the disease progress.

To date most of the MRI studies have used gross anatomical changes to assess neuronal degeneration. It has become clear that MRI can detect cytoarchitectural features of both animals (Aoki et al., 2004, Silva et al., 2008) and human (Duyn et al., 2007) brains. Indeed, hippocampal laminar structural changes using high resolution images in AD and MCI human patients compared to healthy patients have recently been used to detect changes in AD pathology (Kerchner et al., 2010, Mueller et al., 2010, Wisse et al., 2014).

Manganese enhanced MRI (MEMRI) provides a unique contrast in the rodent brain. Following systemic administration of manganese, it can detect, *in vivo*, layers in different areas of the brain, including OB, cortex, hippocampus and cerebellum (Watanabe et al.,

2002, Aoki et al., 2004, Lee et al., 2005, Silva et al., 2008). MEMRI can also highlight discrete anatomical features such as individual glomeruli in the OB (Chuang et al., 2010).

In this study, MEMRI was used to follow the progression of neuronal pathology and its recovery in a reversible olfactory based amyloid induced AD transgenic mouse model. This enables direct tracking of neurodegeneration and its recovery through non-invasive, *in vivo* measurements. Since OSNs regenerate continuously and project their axons directly to OB glomeruli, a particular focus was given to the glomerular layer. Using this model we demonstrated the ability of MEMRI to detect laminar specific changes in the olfactory bulb during APP induced neurodegeneration and its recovery. This work demonstrates that laminar specific measurements by MRI can add information about neurodegeneration, and should enable MRI to assess therapeutic strategies by evaluating olfactory structures in this and possibly other mouse models of APP induced degeneration.

Material and methods

Transgenic mouse line

The transgenic mouse model we used selectively overexpress humanized APP in mature OSNs using olfactory marker protein (OMP) under tetracycline transactivators (tTA) control, as previously described (Nguyen et al., 2007). The tetracycline transactivation system (tet-off) allows spatial and temporal control of transgene expression with the addition of doxycycline (Dox) turning-off promoter function. TetO-hAPP line contains the hAPP transgene (humanized Aβ-domain with familial AD mutations KM570, 571NL "Swedish" and V617F "Indiana") (Jankowsky et al., 2005). OMP-tTA line expresses the tetracycline transactivator in mature OSNs (Yu et al., 2004, Nguyen et al., 2007). OMP-tTA line was crossed with tetO-hAPP line to generate the OMP-hAPP line that selectively expresses hAPP in mature OSNs driven by the OMP promoter. The hAPP overexpression presumably begins during embryonic development when the OMP promoter is activated. Genotyping was performed to recognize mutants containing both tTA and tetO transgenes, while littermates containing only tetO-hAPP transgene were selected as controls. At the ages used in the study (3-8 week old), OMP-hAPP mice did not display extracellular plaques (Cheng et al., 2011). All mice were of mixed (129 × C57BL/6) background and both sexes were used in the study.

Animals were also crossed with OMP-GFP mice to generate tetO-hAPP and OMP-hAPP lines with GFP labeled mature OSNs and their axons. OMP-GFP mice were used to reveal mature OSNs and their axons by fluorescence imaging, since mature OSNs express GFP driven by the OMP promoter at high levels in these mice (Potter et al., 2001).

Turning off hAPP overexpression

Doxycycline containing chow (Dox-chow; 6 g/kg, 0.5 inch pellets, Bio-Serv) was fed to OMP-hAPP mice from 3 or 4 weeks of age for a period of 1 or 3 weeks. Dox prevents the tTA protein from binding to the tetO-sequence, which turns off hAPP expression.

Antibody treatment

hAPP antibody stock (6E10, Covance) was diluted 1:1 with glycerol and kept in −20°C. Just before the treatment, desired amount of antibody stock was taken out and diluted 1:1 with 0.9% NaCl (final antibody concentration: 0.25 mg/ml). Total volume of 3 μl was administered directly to the right naris of each animal from 3 or 4 weeks of age, every day, for a period of either 1 or 3 weeks. Intranasal administration was shown to deliver the hAPP antibody as well as insulin like growth factor into the brain (Thorne et al., 2004, Chauhan et al., 2011). For vehicle treated animals, vehicle consists of 0.75 μl glycerol and 2.25 μl 0.9% NaCl was administrated in the same manner as antibody.

Animal procedure

All animal experiments were performed in accordance to the NIH guidelines and were approved by the Animal Care and Use Committee of the National Institute of Neurological Disorder and Stroke, National Institutes of Health (Bethesda, MD USA). Two age groups, 3 to 4 week and 6 to 8 week old tetO-hAPP and OMP-hAPP mice (BW = 11-25 gr) were used in this study. TetO-hAPP mice of both age groups (n=4 and n=8, respectively) served as control, while OMP-hAPP mice (n=4 for each age group) served as mutant. For neuronal recovery experiment (turning off hAPP overexpression), OMP-hAPP mice fed with Dox containing chow for 1 week, (n=4, 3 to 4 week old) or for 3 weeks (n=5, 6 to 8 week old) were used. For antibody treatment, OMP-hAPP mice were either treated with vehicle (n=4) or with hAPP antibody for 1 week (n=5) or for 3 weeks (n=5).

For manganese enhanced MRI, 100 mM of isotonic $MnCl_2$ (Sigma-Aldrich) solution was infused into the tail vein using a syringe pump (Cole-Parmer Instrument) at a dose of 88 mg/kg and an infusion rate of 0.25 ml/h (total infusion time of ~20 min). During the infusion, mice were anesthetized with 1-2% isoflurane (1:4 air:oxygen mixture) and their body temperature was maintain by a heated water pad. After infusion, mice were returned to the cage and were monitored until fully awake. No abnormalities were observed after infusion in all mice. MRI scanning was performed 24h after manganese administration. Animals were anesthetized with 1.2-2% isoflurane using a nose cone, and their body temperature maintained at 37°C by a heated water bath.

MRI acquisition

Images were acquired on an 11.7T /31cm horizontal bore magnet (Agilent, Oxford, UK), interfaced to an Avance III console (Bruker Biospin, Billerica, MA). A custom build 9 cm diameter birdcage coil was used for homogeneous RF transmission and a small surface coil, 6 mm in diameter, placed on the area of the OB, was used during acquisition. Manganese enhanced MRI images were acquired using a 3D T_1 weighted fast low angle shot (FLASH) sequence, at 50 μm isotropic resolution, with TR/TE = 40/4.4 ms, 25° pulse, bandwidth = 50 kHz, FOV = 12.8×12.8×7.4 mm^3, matrix size = 256×256×148, number of averages = 2, and total scan time of 50 min.

Data analysis

OB volume for each mouse was measured from the MRI images using Medical Image Processing, Analysis, and Visualization (MIPAV) software (NIH; http://mipav.cit.nih.gov).

Measurements were done by manually segmenting both bulbs and calculating the volume. For the antibody treated mice the volume of each OB was measured separately. The average volume and standard deviation was calculated for each group. Statistical analysis was performed using unpaired student's t-test, assuming two tailed distribution, with statistical significance defined as $p < 0.05$.

Intensity profiles across the OB layers, from lateral to medial side, were drawn in horizontal sections that show all layers of the OB in T_1 weighted images using MIPAV. For each mouse, in both bulbs, intensity line profiles were drawn for 4-5 consecutive lines in 3 consecutive slices, for a total of 12-15 lines. Those lines were later aligned by the minimum intensity in the center of the bulb and averaged, to serve as the intensity profile for each mouse. Intensity profile normalization was performed by dividing the intensity profile by its minimum intensity, at the center of the OB. For group analysis the intensity profiles for all the olfactory bulbs of the mice in the group were aligned by the minimum intensity at the center of the bulb and averaged. The intensity profile in antibody treated mice was measured separately for each OB (right and left) in the same manner as described above. Layer to minimum ratio was calculated by dividing the intensity at the peak of both glomerular layer and mitral cell layer at each side (lateral or medial) of the OB by the minimum intensity between the two layers. Statistical analysis was performed using unpaired student's t-test, assuming two tailed distribution, with statistical significance defined as $p < 0.05$.

Whole-mount imaging of GFP labeled OSN axons and glomeruli in the OB

Animals were sacrificed and the brains were rapidly dissected and immersed in PBS. The dorsal surface of the OB was imaged in a Z-stack using confocal microscopy (LSM510, Carl Zeiss). The stack of images was then collapsed into a single frame.

Immunohistochemistry

Fluorescence immunohistochemistry on OB sections was performed as previously described (Cummings and Belluscio, 2010). Primary antibodies included the following: OMP, 1:5000 (Wako); vesicular glutamate transporter 2 (VGlu2), 1:1000 (Millipore). Sections were examined using confocal microscopy (LSM510, Carl Zeiss).

Results

Representative MEMRI images of both coronal and horizontal sections of the OB are shown in Fig. 1a for a 4 week old control (tetO-hAPP) mouse. One day following manganese administration, the different layers in the OB were clearly detected, with higher enhancement for the glomerular and mitral cell layers, as previously reported (Aoki et al., 2004, Lee et al., 2005, Chuang et al., 2010). Some round spots with high intensity could also be observed within the glomerular layer (shown by the black arrows), which likely correspond to individual glomeruli, as was previously reported (Chuang et al., 2010).

Mutant (OMP-hAPP) mice that selectively overexpress hAPP in mature OSNs resulted in the degeneration of the OSNs, already by 3 weeks of age (Cheng et al., 2011, Cheng et al., 2013). Fig. 1b shows the representative MEMRI images of OB for 4 week old mutant mouse. Compared to control mice, the mutant mice showed a different shape and size of the

OB and a decrease in manganese enhancement of the glomerular layer that can be readily detected, as seen in the images (Fig.1a,b). Measurements of OB volumes showed a significant decrease of ~50% in volume for the mutant mice olfactory bulbs compare to control (Table 1). This is consistent with the alteration of the OB structure previously reported (Cheng et al., 2013) for the mutant mice using histological methods.

Intensity line profiles for the individual mice (control and mutant) were drawn across the OB layers, from the lateral to medial side, as shown by the arrows in Fig. 1c. For the control mouse, the normalized intensity profile showed higher manganese enhancement in locations that correspond to the glomerular and mitral cell layers. However, a much smaller manganese enhancement for the glomerular layer was observed for the mutant mouse, while the mitral cell layer was still evident. In addition, the region assigned to the olfactory nerve layer in the control mouse was much smaller in the mutant mouse. The group intensity profile for all mice in the 3 to 4 week old control and mutant groups are shown in Fig. 1d. The group intensity profiles show the average (± sd) of both the left and right OB across all mice in the group (e.g. total of 8 OB in group of 4 mice). Intensity profiles for both the right and left bulbs were not significantly different to the individual sides profiles for both control and mutant mice (Fig. 1c,d), and therefore were graphed together for all further analysis. For both groups, the MRI intensity ratio of the peak of each layer to the minimum intensity of the lateral and medial side was analyzed for the glomerular layer and the mitral cell layer. Both glomerular and mitral cell layers showed a significant decrease in manganese enhancement for the mutant mice compared to the control, with a larger decrease for the glomerular layer (Table 1). Measurements of the distance between the mitral cell layer on the lateral side of the OB to that on the medial side showed a significant increase for mutant mice (0.70 ± 0.06 mm) compared to control mice (0.42 ± 0.03 mm) (Table 1). This can be due to a small increase in the volume of the olfactory ventricle, together with the change in OB shape, for the mutant mice, as can also be seen in the MEMRI images by the dark area in the middle of the bulbs (Fig. 1a,b).

To test whether MEMRI can detect the progression of the neuronal changes in this AD mouse model, we further imaged a group of 6 to 8 weeks old mice. Similar to the 3 to 4 week old mice, the laminar structure of control OB is readily observed by MEMRI in older control mice (Fig. 2a,e) and a decrease in manganese enhancement of the glomerular layer was observed in the older mutant mice (Fig. 2b,f). A ~50% decrease in OB volume for mutant mice compared to control mice was also measured for the 6 to 8 weeks old mice (Table 2).

The hAPP overexpression can be turned off by feeding mutant mice with doxycycline containing chow, as previously described (Cheng et al., 2011). After only 1 week of turning off hAPP overexpression in 3 week old mice, a significant increase in manganese enhancement of the glomerular layer was observed compared to mutant mice without Dox treatment, as seen in Fig. 2b,c. The shape of the OB was also changed and was more similar to the OB of control mice than to that of mutant mice. However, no significant increase of OB volume was measured after 1 week of doxycycline, compared to mutant mice at the same age group of 3 to 4 weeks old mice (Table 2). Hence, laminar enhancement increase precedes the recovery of OB size. Turning off hAPP overexpression for two additional

weeks, as seen in Fig. 2g, showed a further recovery of the OB shape and higher manganese enhancement of the glomerular layer compared to the age matched control and mutant groups (Fig. 2e,f) and compared to 1 week of the doxycycline treatment group (Fig. 2c). Increase in OB volume, after 3 weeks of doxycycline treatment, indicated that the OB continued to grow but did not reach the same volume as control mice at the same age (Table 2). These imaging results are consistent with previously reported histological studies (Cheng et al., 2013) that showed a partial recovery of the OB shape after 1 week of doxycycline treatment with an incomplete restoration of the glomerular layer and reappearance of glomeruli when compared to mutant mice.

The corresponding group intensity profiles for all groups of mice are shown in Fig. 2d and h. With only one week of doxycycline treatment the manganese enhancement of the glomerular layer increased and the intensity profile was more similar to the intensity profile of control mice, than to that of mutant mice, with a lower intensity area that can be assigned to the olfactory nerve layer, which indicates recovery of this layer of the bulb. The manganese enhancement in the glomerular layer was further increased by 3 weeks of doxycycline treatment, resulting in an even greater similarity of the intensity profile to that of the control mice. The combined layer to minimum ratio for both glomerular and mitral cell layers showed a significant decrease in manganese enhancement, with a slightly larger decrease for the glomerular layer, for mutant mice of both age groups compared to control mice at the same age. The layer to minimum ratio showed a significant increase in manganese enhancement of the glomerular layer by 3 weeks of doxycycline treatment, but was not significant after only 1 week of doxycycline treatment (Table 2). The distance between the lateral and medial sides of the mitral cell layer was significantly larger for the mutant mice compared to control mice (in both age groups). This distance was significantly reduced already after 1 week of doxycycline treatment and decreased further after 3 weeks of treatment, to become similar to that in control mice (Table 2). This is due to the changes in the OB shape that was more similar to that of the control mice, together with a possible decrease in olfactory ventricle volume, as can be seen in the MEMRI images (Fig. 2).

To test if an antibody against APP could reverse the effect of hAPP overexpression, MEMRI was used. This is of interest because antibody trials have been the focus of different clinical trials for subjects with AD, so far with little success (Vellas et al., 2013). Representative MEMRI images of mutant mice that received antibody treatment are shown in Fig. 3. hAPP antibody administration to the right naris of control mice (Fig. 3a), did not change the manganese enhancement in the different layers or the OB shape and size of the right side compared to the untreated left side and to control mice (Fig. 1 and 2). This was expected as antibody treatment should not have any effect in control mice. Similarly, vehicle administration to the right naris in mutant mice did not cause any changes in OB shape and size and manganese layer enhancement when compared to the left side and to mutant mice groups (Fig. 3b, Fig. 1 and 2). The group intensity profiles across both OB from the lateral side of the left bulb to the lateral side of the right bulb were also similar to those of the control and untreated mutant mice (Fig. 3e). After 1 week of hAPP antibody administration to the right naris, a small increase in manganese enhancement of the glomerular layer was observed in the MEMRI image for the right OB compared to the left OB (Fig. 3c, arrow). This can also be seen in the group intensity profile across bulbs, where a very small increase

in manganese enhancement in the right bulb was observed (Fig. 3e, arrow). After 3 weeks of hAPP antibody treatment, a higher increase in manganese enhancement of the glomerular layer was seen in the right bulb, with no change in the left bulb compare to mutant mice without any treatment (Fig. 3d, arrow). The group intensity profile showed an increase in glomerular layer enhancement, but this did not reach statistical significance of $p < 0.05$ (Fig. 3e, arrow). The layer to minimum ratio of the glomerular and mitral cell layers of the right OB increased after 3 weeks of hAPP antibody administration but was not significantly different when compared to the right OB in mutant mice (Table 3). However, for the glomerular layer this increase was significant when compared to the untreated left OB ($p < 0.01$). The increase in manganese enhancement was smaller for the hAPP antibody administration mice when compared to that of the doxycycline treatment mice at the same time points, and may indicate that more treatment time is needed when using an antibody.

The distance between the lateral and medial sides of the mitral cell layer of the right OB did not show a decrease even after 3 weeks of hAPP antibody administration, and was similar to that of the left OB and those of untreated mutant mice. Moreover, the volumes of the left and right bulbs did not show any significant difference between the treated and untreated side and between the treated and untreated mutant mice (Table 3). Therefore, the only indication for the effectiveness of hAPP antibody treatment was the small, but not statistically significant, increase in manganese enhancement in the glomerular layer as can be seen in the MEMRI image and the intensity profiles. Thus, hAPP antibody treatment in these mice was not a robust therapy option, especially compared to inhibiting hAPP expression with doxycycline.

We further tested if the small increase in manganese enhancement in the glomerular layer observed after hAPP antibody treatment corresponded to any anatomical changes detectable by histological methods. Animals were crossed with OMP-GFP mice to generate both control and mutant mice with GFP labeled mature OSNs and their axons. Whole-mount fluorescence imaging showed a large amount of axon bundles from OSNs innervating the OB and terminating in numerous glomeruli in control animals, whereas in the mutant animals sparse GFP-positive axons and only sparse glomeruli were observable. After 3 weeks of treatment with hAPP antibody, more axons and glomeruli were detected in the OB of mutant animals. However, the fluorescence was much dimmer and the glomeruli much smaller than that in the control (Fig. 4a). Immunohistochemical staining on OB sections also revealed a small recovery of the glomerular structure after hAPP antibody treatment. Similar to previous findings (Cheng et al., 2013), the mutant animals treated with vehicle, demonstrated a dramatic loss of OMP-positive axons and glomeruli compared to controls, as well as a clear reduction in VGlu2 signal, a relatively specific marker for OSN axon terminals in the OB. After 3 weeks of hAPP antibody treatment more OMP-positive axons and glomeruli filled with both OMP and VGlu2 - positive axon terminals remained (Fig. 4c). However, the lack of recovery of anatomical features for MRI indicates those effects must have been small for the entire bulb.

Discussion

This study demonstrates the ability of MRI to detect laminar specific anatomical changes associated with both APP-induced neurodegeneration and recovery, *in vivo*, in an olfactory based amyloid induced AD mouse model. To get contrast specific olfactory bulb layers we used manganese enhanced MRI. Many papers have demonstrated that MEMRI can detect many features of cytoarchitecture including hippocampal sub-regions, layers in hippocampus, retina, cortex, as well as layers in the olfactory bulb (Watanabe et al., 2002, Aoki et al., 2004, Lee et al., 2005, Berkowitz et al., 2008, Silva et al., 2008, Nair et al., 2011). Using MEMRI we have shown that overexpression of hAPP in mutant mice results in a disruption of the OB laminar structure and appearance, with reduced manganese enhancement of the glomerular layer and a decrease in OB volume. Turning off hAPP overexpression with doxycycline showed a recovery of the OB structure and an increase in manganese enhancement of the glomerular layer as early as 1 week after and a further recovery after 3 weeks. This study further supports the observations reported in a recent study with this OMP-hAPP mouse model, where already at 3 weeks of age the mutant mice exhibit a rapid disruption of the olfactory circuitry, using anatomical, functional and behavioral analysis. This circuitry disruption was partially restored after turning off hAPP overexpression (Cheng et al., 2013).

The MEMRI images of the mutant mice show a very different shape and size of the OB compare to the control mice, with a ~50% decrease in OB volume compared to controls. One can argue that this difference in appearance can be associated with delayed growth of the OB rather than with degeneration. Although slower growth can be a possibility, previous reported data in this mouse model showed that OSN axons exhibit a strong caspase3 signal in the olfactory nerve layer in the OB, as well as loss of OSNs in the olfactory epithelium that linked hAPP overexpression to neuronal death and neurodegeneration (Cheng et al., 2011, Cheng et al., 2013). Furthermore, our MEMRI images also show an almost complete loss of the olfactory nerve layer together with a significant decrease in manganese enhancement of the glomerular layer in both age groups mutant mice compare to their age matched controls, which support large degeneration of neurons. An earlier MRI study used a double-transgenic APP/tTa mouse model that overexpressed hAPP under the control of CaMKII promoter which is expressed more broadly throughout the brain. The hAPP overexpression was suppressed until 6 weeks of age and then allowed to reactivate which resulted in volume reduction in various brain areas such as hippocampus and cortex that serve as a measure for degeneration (Badea et al., 2010). However, this study lacked any laminar analysis that could provide important insight into the specific cell types that are affected and the resulting loss in connectivity. Thus, it will be interesting to determine if overexpression of hAPP in our mouse model causes similar laminar specific degeneration in fully grown mice by starting the expression of hAPP in adult olfactory neurons after full OB size is achieve.

Overexpression of hAPP causes a large scale apoptosis of OSNs already by 3 weeks of age in which the glomerular layer and the olfactory nerve layer were shown to be much thinner, with a massive loss of glomeruli in the mutant mice compared to control (Cheng et al., 2013). As OSNs project their axons directly to OB glomeruli, this is consistent with the loss

of OSNs that was observed at the olfactory epithelium (Cheng et al., 2011). Here we show that this disruption in OSNs resulted also in a glomerular layer with a lower manganese enhancement and almost complete elimination of the olfactory nerve layer. This can be attributed to the loss of OSN synaptic input and massive loss of glomeruli in the glomerular layer. The distribution of manganese in the brain following iv administration is not well understood and can be effected by many factors. In the OB, there is more than one mechanism that contributes to the manganese enhancement. Manganese first enters the OB from the CSF surrounding the bulb. Mn^{2+} can also trace into the bulb along OSNs from the turbinates as well as from other brain areas. The manganese distribution and level of enhancement also depends on different manganese transporter mechanisms, the cell density and type of cells, and might be influenced by the activity in an area (Aoki et al., 2004, Lee et al., 2005). The loss of OSNs and their projections to the glomeruli resulted in decreased ability to uptake manganese into the glomerular layer in the OB, but the specific mechanism is unknown. Lower uptake and transfer due to loss of OSNs is a likely contributor and direct administration of manganese into the nostrils will enable a better understanding of whether this is an important factor that contributes to the decreased uptake. With the increased restoration of the glomerular layer and the amount of glomeruli following doxycycline administration an increase in manganese enhancement of the glomerular layer was evident. This suggests that the glomeruli are important for manganese accumulation in the layer, consistent with a report that showed detection of individual glomeruli with MEMRI, due to increased Mn^{2+} uptake by glomeruli (Chuang et al., 2010). Interestingly, glomeruli are mostly made up of synaptic connections between OSN and mitral cells, indicating that manganese is accumulating in structures that are able to alter contrast in MEMRI. Furthermore, our results demonstrate that mitral synaptic cells are still present, indicating that presynaptic accumulation of Mn^{2+} in OSN contributes significantly to glomerular enhancement. Using this mouse model in future studies, it should be possible to learn more about the detailed cellular mechanisms that are responsible for controlling manganese distribution in the OB following iv administration.

Many studies have used MRI to image plaque formation in animal models of AD that overexpress APP (Wadghiri et al., 2003, Helpern et al., 2004, Jack et al., 2004a, Zhang et al., 2004). However, most studies are able to image plaque formation that is only detectable at late stages of AD. Because olfactory dysfunction is an early symptom of AD there is an increased interest in imaging these early changes in the olfactory system. The Tg2576 Alzheimer's mouse model is shown to exhibit Aβ depositions in the OB earlier than in other brain regions, with a decrease in olfactory function (Wesson et al., 2010, Wesson et al., 2011). This animal model was later used to measure axonal transport rates into the OB using MEMRI (Smith et al., 2007, Wang et al., 2012). Following Mn^{2+} administration to the mice nostrils, the rates of manganese transport from the OSNs to the OB layers were calculated and showed a decrease in transport rates during progression of Aβ accumulation (Smith et al., 2007). It will be interesting to see if the anatomical features reported in the present study will apply to other animal models. Future studies will utilize the transport of manganese from the nose into the OB to study the disruption in OB circuitry as previously observed in the OMP-hAPP model (Cheng et al., 2011, Cheng et al., 2013).

APP antibody results showed a trend toward recovery with a small increase in manganese enhancement of the glomerular layer in the right side (treated side), which reached statistical significance only when compared to the left side (untreated) but not when compared to mutant mice. This leads us to conclude that binding only the extracellular Aβ is ineffective by itself at blocking APP induced cell death, and thus might not be the best approach for the treatment of AD progression. Interestingly, this is consistent with recent clinical trials (Vellas et al., 2013) that targeted extracellular Aβ as a therapeutic strategy, which only showed a weak beneficial effect. MEMRI can be used to evaluate whether other reagents such as insulin (Craft et al., 2012) can block neuronal loss. For the present study doxycycline and antibody treatments give a range of results from little to almost complete recovery of the deficit in the OB.

In this study we used different quantitative measurements to evaluate the changes in the OB for neurodegeneration and recovery: the OB volume, manganese intensity for the different layers and the distance between the mitral cell layer on the lateral side to that on the medial side – a measure for shape changes of the bulb. The most prominent changes were in the OB volume, enhancement of the glomerular layer, and in the distance between mitral cell layers of both sides of the bulb during degeneration and recovery. Significant reduction in OB volume was previously reported in different MRI studies of neurological disorders such as AD, Parkinson's disease, depression and schizophrenia, that correlates with the disease progression (Turetsky et al., 2000, Thomann et al., 2009, Negoias et al., 2010, Wang et al., 2011). Increase in OB volume was shown following 3 weeks of doxycycline treatment in the present model. Interestingly, an increase in OB volume was reported following treatment in chronic sinonasal disease in humans (Gudziol et al., 2009). Therefore, OB volume changes can be a sensitive measure to assess degeneration and recovery when using different pharmacological reagents. This is also similar to hippocampal volume measurements used in human AD studies where reduction in total hippocampal volume was observed for AD and MCI patients (Jack et al., 2004b, Ridha et al., 2008). Moreover, human studies with high magnetic field MRI were able to detect hippocampal subfields and measure their volume in AD and MCI subjects. AD patients compared to MCI and healthy patients showed a much smaller volume of subfields such as the subiculum, CA1, CA3 and dentate gyrus (DG) (Kerchner et al., 2010, Mueller et al., 2010, Wisse et al., 2014). As hippocampal changes are measures for AD, it would be of interest to detect changes in laminar structure of the hippocampus in a transgenic mouse model of AD with hippocampal pathology. The changes in the distance between the mitral cell layers in both sides of the bulb also show a correlation to the degeneration level with an increase in distance. This is a result of changes in the OB shape in mutant mice, but can also suggest a small ventricle volume increase as can be seen qualitatively in the MEMRI images, which can be similar to reported ventricle enlargement in studies of AD and MCI patients (Thompson et al., 2004, Tang et al., 2014). However, the possible increase in the ventricular volume need to be quantitatively measured in future studies. Similarly, it would be interesting to measure laminar changes in human olfactory bulb as a potential marker for AD progression. Susceptibility weighted MRI that was shown to be very useful for imaging cytoarchitecture in the brain (Duyn et al., 2007, Shmueli et al., 2009) and T_1 changes that have been used to detect olfactory layers, without the need of a contrast agent in rodents (Yang et al., 1998), can be used.

This study is one of a very few studies that were able to follow laminar specific structural changes in animal models of degeneration, using *in vivo* MRI. Changes in laminar structure of the retina together with retinal thinning were detected in a retinal degeneration animal model using MEMRI (Berkowitz et al., 2008, Nair et al., 2011). In αCaMkII HKO mice, a model for psychiatric illness, a lower manganese enhancement in the DG and a higher enhancement in the CA1 in the hippocampus were observed compared to control mice (Hattori et al., 2013). In human studies with high magnetic field, MRI was able to detect hippocampal subfields in AD and MCI subjects and showed a reduction in several subfield volumes, such as the subiculum, CA1, CA3 and DG, compared to healthy patients (Kerchner et al., 2010, Mueller et al., 2010, Wisse et al., 2014). However, to the best of our knowledge, this study is the first to follow laminar changes not only during neurodegeneration but also during recovery, *in vivo*, with high resolution MRI. It is likely that using high resolution MRI to study cytoarchitecture changes will increase the sensitivity and specificity to imaging studies of degeneration and will be useful for identifying therapeutic options. As olfactory dysfunction is an early symptom of AD, the ability to detect early changes and develop potential therapeutics in the olfactory system is of great importance. Here we demonstrated that MEMRI can detect specific anatomical changes associated with both APP-induced neurodegeneration and recovery in the OB and that this method can be used to assess the ability of different pharmacological reagents to block olfactory neuronal loss and can serve as a unique *in vivo* screening tool to both identify potential therapeutics for olfactory neuronal loss and test their efficacy.

Acknowledgments

This research was supported by the Intramural Research Program of the NIH, NINDS. We thank Nadia Bouraoud and Li Bai for assistance with animal procedures and animal handling. We also thank Dr. Steve Dodd for providing MRI technical support.

References

Aoki I, Wu YJ, Silva AC, Lynch RM, Koretsky AP. In vivo detection of neuroarchitecture in the rodent brain using manganese-enhanced MRI. NeuroImage. 2004; 22:1046–1059. doi: 10.1016/j.neuroimage.2004.03.031. [PubMed: 15219577]

Arnold SE, Lee EB, Moberg PJ, Stutzbach L, Kazi H, Han LY, Lee VM, Trojanowski JQ. Olfactory epithelium amyloid-beta and paired helical filament-tau pathology in Alzheimer disease. Annals of neurology. 2010; 67:462–469. doi: 10.1002/ana.21910. [PubMed: 20437581]

Bacon AW, Bondi MW, Salmon DP, Murphy C. Very early changes in olfactory functioning due to Alzheimer's disease and the role of apolipoprotein E in olfaction. Annals of the New York Academy of Sciences. 1998; 855:723–731. doi. [PubMed: 9929677]

Badea A, Johnson GA, Jankowsky JL. Remote sites of structural atrophy predict later amyloid formation in a mouse model of Alzheimer's disease. NeuroImage. 2010; 50:416–427. doi: DOI 10.1016/j.neuroimage.2009.12.070. [PubMed: 20035883]

Berkowitz BA, Gradianu M, Schafer S, Jin Y, Porchia A, Iezzi R, Roberts R. Ionic dysregulatory phenotyping of pathologic retinal thinning with manganese-enhanced MRI. Investigative ophthalmology & visual science. 2008; 49:3178–3184. doi: 10.1167/iovs.08-1720. [PubMed: 18362105]

Calof AL, Hagiwara N, Holcomb JD, Mumm JS, Shou J. Neurogenesis and cell death in olfactory epithelium. Journal of neurobiology. 1996; 30:67–81. doi: 10.1002/(SICI)1097-4695(199605)30:1<67::AID-NEU7>3.0.CO;2-E. [PubMed: 8727984]

Chauhan NB, Davis F, Xiao C. Wheat germ agglutinin enhanced cerebral uptake of anti-A beta antibody after intranasal administration in 5XFAD mice. Vaccine. 2011; 29:7631–7637. doi: DOI 10.1016/j.vaccine.2011.08.009. [PubMed: 21840361]

Cheng N, Bai L, Steuer E, Belluscio L. Olfactory functions scale with circuit restoration in a rapidly reversible Alzheimer's disease model. The Journal of neuroscience: the official journal of the Society for Neuroscience. 2013; 33:12208–12217. doi: 10.1523/JNEUROSCI.0291-13.2013. [PubMed: 23884929]

Cheng N, Cai H, Belluscio L. In vivo olfactory model of APP-induced neurodegeneration reveals a reversible cell-autonomous function. The Journal of neuroscience: the official journal of the Society for Neuroscience. 2011; 31:13699–13704. doi: 10.1523/JNEUROSCI.1714-11.2011. [PubMed: 21957232]

Chuang KH, Belluscio L, Koretsky AP. In vivo detection of individual glomeruli in the rodent olfactory bulb using manganese enhanced MRI. NeuroImage. 2010; 49:1350–1356. doi: 10.1016/j.neuroimage.2009.09.060. [PubMed: 19800011]

Craft S, Baker LD, Montine TJ, Minoshima S, Watson GS, Claxton A, Arbuckle M, Callaghan M, Tsai E, Plymate SR, Green PS, Leverenz J, Cross D, Gerton B. Intranasal Insulin Therapy for Alzheimer Disease and Amnestic Mild Cognitive Impairment A Pilot Clinical Trial. Arch Neurol-Chicago. 2012; 69:29–38. doi: DOI 10.1001/archneurol.2011.233. [PubMed: 21911655]

Cummings DM, Belluscio L. Continuous Neural Plasticity in the Olfactory Intrabulbar Circuitry. Journal of Neuroscience. 2010; 30:9172–9180. doi: Doi 10.1523/Jneurosci.1717-10.2010. [PubMed: 20610751]

Dubois B, Feldman HH, Jacova C, Cummings JL, DeKosky ST, Barberger-Gateau P, Delacourte A, Frisoni G, Fox NC, Galasko D, Gauthier S, Hampel H, Jicha GA, Meguro K, O'Brien J, Pasquier F, Robert P, Rossor M, Salloway S, Sarazin M, de Souza LC, Stern Y, Visser PJ, Scheltens P. Revising the definition of Alzheimer's disease: a new lexicon. Lancet Neurol. 2010; 9:1118–1127. doi: Doi 10.1016/S1474-4422(10)70223-4. [PubMed: 20934914]

Duyn JH, van Gelderen P, Li TQ, de Zwart JA, Koretsky AP, Fukunaga M. High-field MRI of brain cortical substructure based on signal phase. Proceedings of the National Academy of Sciences of the United States of America. 2007; 104:11796–11801. doi: 10.1073/pnas.0610821104. [PubMed: 17586684]

Farbman AI. Olfactory neurogenesis: genetic or environmental controls? Trends in neurosciences. 1990; 13:362–365. doi: 10.1016/0166-2236(90)90017-5. [PubMed: 1699323]

Gudziol V, Buschhuter D, Abolmaali N, Gerber J, Rombaux P, Hummel T. Increasing olfactory bulb volume due to treatment of chronic rhinosinusitis-a longitudinal study. Brain. 2009; 132:3096–3101. doi: Doi 10.1093/Brain/Awp243. [PubMed: 19773353]

Hardy J, Selkoe DJ. The amyloid hypothesis of Alzheimer's disease: progress and problems on the road to therapeutics. Science. 2002; 297:353–356. doi: 10.1126/science.1072994. [PubMed: 12130773]

Hattori S, Hagihara H, Ohira K, Aoki I, Saga T, Suhara T, Higuchi M, Miyakawa T. In vivo evaluation of cellular activity in alphaCaMKII heterozygous knockout mice using manganese-enhanced magnetic resonance imaging (MEMRI). Frontiers in integrative neuroscience. 2013; 7:76. doi: 10.3389/fnint.2013.00076. [PubMed: 24273499]

Helpern JA, Lee SP, Falangola MF, Dyakin VV, Bogart A, Ardekani B, Duff K, Branch C, Wisniewski T, de Leon MJ, Wolf O, O'Shea J, Nixon RA. MRI assessment of neuropathology in a transgenic mouse model of Alzheimer's disease. Magnetic resonance in medicine: official journal of the Society of Magnetic Resonance in Medicine / Society of Magnetic Resonance in Medicine. 2004; 51:794–798. doi: 10.1002/mrm.20038.

Jack CR, Albert MS, Knopman DS, McKhann GM, Sperling RA, Carrillo MC, Thies B, Phelps CH. Introduction to the recommendations from the National Institute on Aging-Alzheimer's Association workgroups on diagnostic guidelines for Alzheimer's disease. Alzheimers & Dementia. 2011; 7:257–262. doi: DOI 10.1016/j.jalz.2011.03.004.

Jack CR Jr. Garwood M, Wengenack TM, Borowski B, Curran GL, Lin J, Adriany G, Grohn OH, Grimm R, Poduslo JF. In vivo visualization of Alzheimer's amyloid plaques by magnetic resonance imaging in transgenic mice without a contrast agent. Magnetic resonance in medicine:

official journal of the Society of Magnetic Resonance in Medicine / Society of Magnetic Resonance in Medicine. 2004a; 52:1263–1271. doi: 10.1002/mrm.20266.

Jack CR, Shiung MM, Gunter JL, O'Brien PC, Weigand SD, Knopman DS, Boeve BF, Ivnik RJ, Smith GE, Cha RH, Tangalos EG, Petersen RC. Comparison of different MRI brain atrophy, rate measures with clinical disease progression in AD. Neurology. 2004b; 62:591–600. doi. [PubMed: 14981176]

Jankowsky JL, Slunt HH, Gonzales V, Savonenko AV, Wen JC, Jenkins NA, Copeland NG, Younkin LH, Lester HA, Younkin SG, Borchelt DR. Persistent amyloidosis following suppression of Abeta production in a transgenic model of Alzheimer disease. PLoS medicine. 2005; 2:e355. doi: 10.1371/journal.pmed.0020355. [PubMed: 16279840]

Kerchner GA, Hess CP, Hammond-Rosenbluth KE, Xu D, Rabinovici GD, Kelley DAC, Vigneron DB, Nelson SJ, Miller BL. Hippocampal CA1 apical neuropil atrophy in mild Alzheimer disease visualized with 7-T MRI. Neurology. 2010; 75:1381–1387. doi. [PubMed: 20938031]

Klunk WE, Engler H, Nordberg A, Wang Y, Blomqvist G, Holt DP, Bergstrom M, Savitcheva I, Huang GF, Estrada S, Ausen B, Debnath ML, Barletta J, Price JC, Sandell J, Lopresti BJ, Wall A, Koivisto P, Antoni G, Mathis CA, Langstrom B. Imaging brain amyloid in Alzheimer's disease with Pittsburgh Compound-B. Annals of neurology. 2004; 55:306–319. doi: 10.1002/ana.20009. [PubMed: 14991808]

Lee JH, Silva AC, Merkle H, Koretsky AP. Manganese-enhanced magnetic resonance imaging of mouse brain after systemic administration of MnCl2: dose-dependent and temporal evolution of T1 contrast. Magnetic resonance in medicine: official journal of the Society of Magnetic Resonance in Medicine / Society of Magnetic Resonance in Medicine. 2005; 53:640–648. doi: 10.1002/mrm.20368.

Mueller SG, Schuff N, Yaffe K, Madison C, Miller B, Weiner MW. Hippocampal Atrophy Patterns in Mild Cognitive Impairment and Alzheimer's Disease. Human brain mapping. 2010; 31:1339–1347. doi: Doi 10.1002/Hbm.20934. [PubMed: 20839293]

Nair G, Pardue MT, Kim M, Duong TQ. Manganese-Enhanced MRI Reveals Multiple Cellular and Vascular Layers in Normal and Degenerated Retinas. J Magn Reson Imaging. 2011; 34:1422–1429. doi: Doi 10.1002/Jmri.22719. [PubMed: 21964629]

Negoias S, Croy I, Gerber J, Puschmann S, Petrowski K, Joraschky P, Hummel T. Reduced Olfactory Bulb Volume and Olfactory Sensitivity in Patients with Acute Major Depression. Neuroscience. 2010; 169:415–421. doi: DOI 10.1016/j.neuroscience.2010.05.012. [PubMed: 20472036]

Nguyen MQ, Zhou Z, Marks CA, Ryba NJ, Belluscio L. Prominent roles for odorant receptor coding sequences in allelic exclusion. Cell. 2007; 131:1009–1017. doi: 10.1016/j.cell.2007.10.050. [PubMed: 18045541]

Potter SM, Zheng C, Koos DS, Feinstein P, Fraser SE, Mombaerts P. Structure and emergence of specific olfactory glomeruli in the mouse. The Journal of neuroscience: the official journal of the Society for Neuroscience. 2001; 21:9713–9723. doi. [PubMed: 11739580]

Ridha BH, Anderson VM, Barnes J, Boyes RG, Price SL, Rossor MN, Whitwell JL, Jenkins L, Black RS, Grundman M, Fox NC. Volumetric MRI and cognitive measures in Alzheimer disease - Comparison of markers of progression. J Neurol. 2008; 255:567–574. doi: DOI 10.1007/s00415-008-0750-9. [PubMed: 18274807]

Rowe CC, Ackerman U, Browne W, Mulligan R, Pike KL, O'Keefe G, Tochon-Danguy H, Chan G, Berlangieri SU, Jones G, Dickinson-Rowe KL, Kung HP, Zhang W, Kung MP, Skovronsky D, Dyrks T, Hall G, Krause S, Friebe M, Lehman L, Lindemann S, Dinkelborg LM, Masters CL, Villemagne VL. Imaging of amyloid beta in Alzheimer's disease with F-18-BAY94-9172, a novel PET tracer: proof of mechanism. Lancet Neurol. 2008; 7:129–135. doi: Doi 10.1016/S1474-4422(08)70001-2. [PubMed: 18191617]

Shmueli K, de Zwart JA, van Gelderen P, Li TQ, Dodd SJ, Duyn JH. Magnetic susceptibility mapping of brain tissue in vivo using MRI phase data. Magnetic resonance in medicine: official journal of the Society of Magnetic Resonance in Medicine / Society of Magnetic Resonance in Medicine. 2009; 62:1510–1522. doi: 10.1002/mrm.22135.

Silva AC, Lee JH, Wu CW, Tucciarone J, Pelled G, Aoki I, Koretsky AP. Detection of cortical laminar architecture using manganese-enhanced MRI. Journal of neuroscience methods. 2008; 167:246–257. doi: 10.1016/j.jneumeth.2007.08.020. [PubMed: 17936913]

Smith KD, Kallhoff V, Zheng H, Pautler RG. In vivo axonal transport rates decrease in a mouse model of Alzheimer's disease. NeuroImage. 2007; 35:1401–1408. doi: 10.1016/j.neuroimage.2007.01.046. [PubMed: 17369054]

Talamo BR, Rudel R, Kosik KS, Lee VM, Neff S, Adelman L, Kauer JS. Pathological changes in olfactory neurons in patients with Alzheimer's disease. Nature. 1989; 337:736–739. doi: 10.1038/337736a0. [PubMed: 2465496]

Tang X, Holland D, Dale AM, Younes L, Miller MI, Alzheimer's Disease Neuroimaging I. Shape abnormalities of subcortical and ventricular structures in mild cognitive impairment and Alzheimer's disease: Detecting, quantifying, and predicting. Human brain mapping. 2014; 35:3701–3725. doi: 10.1002/hbm.22431. [PubMed: 24443091]

Thomann PA, Dos Santos V, Toro P, Schnonknecht P, Essig M, Schroder J. Reduced olfactory bulb and tract volume in early Alzheimer's disease-A MRI study. Neurobiol Aging. 2009; 30:838–841. doi: DOI 10.1016/j.neurobiolaging.2007.08.001. [PubMed: 17875348]

Thompson PM, Hayashi KM, de Zubicaray GI, Janke AL, Rose SE, Semple J, Hong MS, Herman DH, Gravano D, Doddrell DM, Toga AW. Mapping hippocampal and ventricular change in Alzheimer disease. NeuroImage. 2004; 22:1754–1766. doi: DOI 10.1016/j.neuroimage.2004.03.040. [PubMed: 15275931]

Thorne RG, Pronk GJ, Padmanabhan V, Frey WH. Delivery of insulin-like growth factor-I to the rat brain and spinal cord along olfactory and trigeminal pathways following intranasal administration. Neuroscience. 2004; 127:481–496. doi: DOI 10.1016/j.neuroscience.2004.05.029. [PubMed: 15262337]

Turetsky BI, Moberg PJ, Yousem DM, Doty RL, Arnold SE, Gur RE. Reduced olfactory bulb volume in patients with schizophrenia. Am J Psychiat. 2000; 157:828–830. doi: DOI 10.1176/appi.ajp.157.5.828. [PubMed: 10784482]

Vandenberghe R, Van Laere K, Ivanoiu A, Salmon E, Bastin C, Triau E, Hasselbalch S, Law I, Andersen A, Korner A, Minthon L, Garraux G, Nelissen N, Bormans G, Buckley C, Owenius R, Thurfjell L, Farrar G, Brooks DJ. 18F-flutemetamol amyloid imaging in Alzheimer disease and mild cognitive impairment: a phase 2 trial. Annals of neurology. 2010; 68:319–329. doi: 10.1002/ana.22068. [PubMed: 20687209]

Vellas B, Carrillo MC, Sampaio C, Brashear HR, Siemers E, Hampel H, Schneider LS, Weiner M, Doody R, Khachaturian Z, Cedarbaum J, Grundman M, Broich K, Giacobini E, Dubois B, Sperling R, Wilcock GK, Fox N, Scheltens P, Touchon J, Hendrix S, Andrieu S, Aisen P, Members EUCTF. Designing drug trials for Alzheimer's disease: what we have learned from the release of the phase III antibody trials: a report from the EU/US/CTAD Task Force. Alzheimer's & dementia: the journal of the Alzheimer's Association. 2013; 9:438–444. doi: 10.1016/j.jalz.2013.03.007.

Wadghiri YZ, Sigurdsson EM, Sadowski M, Elliott JI, Li Y, Scholtzova H, Tang CY, Aguinaldo G, Pappolla M, Duff K, Wisniewski T, Turnbull DH. Detection of Alzheimer's amyloid in transgenic mice using magnetic resonance microimaging. Magnetic resonance in medicine: official journal of the Society of Magnetic Resonance in Medicine / Society of Magnetic Resonance in Medicine. 2003; 50:293–302. doi: 10.1002/mrm.10529.

Wang FH, Appelkvist P, Klason T, Gissberg O, Bogstedt A, Eliason K, Martinsson S, Briem S, Andersson A, Visser SA, Ivarsson M, Lindberg M, Agerman K, Sandin J. Decreased axonal transport rates in the Tg2576 APP transgenic mouse: improvement with the gamma-secretase inhibitor MRK-560 as detected by manganese-enhanced MRI. The European journal of neuroscience. 2012; 36:3165–3172. doi: 10.1111/j.1460-9568.2012.08258.x. [PubMed: 22958226]

Wang J, You H, Liu JF, Ni DF, Zhang ZX, Guan J. Association of Olfactory Bulb Volume and Olfactory Sulcus Depth with Olfactory Function in Patients with Parkinson Disease. Am J Neuroradiol. 2011; 32:677–681. doi: Doi 10.3174/Ajnr.A2350. [PubMed: 21330398]

Watanabe T, Natt O, Boretius S, Frahm J, Michaelis T. In vivo 3D MRI staining of mouse brain after subcutaneous application of MnCl2. Magnet Reson Med. 2002; 48:852–859. doi: Doi 10.1002/Mrm.10276.

Wesson DW, Borkowski AH, Landreth GE, Nixon RA, Levy E, Wilson DA. Sensory network dysfunction, behavioral impairments, and their reversibility in an Alzheimer's beta-amyloidosis

mouse model. The Journal of neuroscience: the official journal of the Society for Neuroscience. 2011; 31:15962–15971. doi: 10.1523/JNEUROSCI.2085-11.2011. [PubMed: 22049439]

Wesson DW, Levy E, Nixon RA, Wilson DA. Olfactory dysfunction correlates with amyloid-beta burden in an Alzheimer's disease mouse model. The Journal of neuroscience: the official journal of the Society for Neuroscience. 2010; 30:505–514. doi: 10.1523/JNEUROSCI.4622-09.2010. [PubMed: 20071513]

Wisse LEM, Biessels GJ, Heringa SM, Kuijf HJ, Koek DL, Luijten PR, Geerlings MI, Impairment UVC. Hippocampal subfield volumes at 7T in early Alzheimer's disease and normal aging. Neurobiol Aging. 2014; 35:2039–2045. doi: DOI 10.1016/j.neurobiolaging.2014.02.021. [PubMed: 24684788]

Yang XJ, Renken R, Hyder F, Siddeek M, Greer CA, Shepherd GM, Shulman RG. Dynamic mapping at the laminar level of odor-elicited responses in rat olfactory bulb by functional MRI. Proceedings of the National Academy of Sciences of the United States of America. 1998; 95:7715–7720. doi: DOI 10.1073/pnas.95.13.7715. [PubMed: 9636216]

Yu CR, Power J, Barnea G, O'Donnell S, Brown HE, Osborne J, Axel R, Gogos JA. Spontaneous neural activity is required for the establishment and maintenance of the olfactory sensory map. Neuron. 2004; 42:553–566. doi. [PubMed: 15157418]

Zhang J, Yarowsky P, Gordon MN, Di Carlo G, Munireddy S, van Zijl PCM, Mori S. Detection of amyloid plaques in mouse models of Alzheimer's disease by magnetic resonance imaging. Magnet Reson Med. 2004; 51:452–457. doi: Doi 10.1002/Mrm.10730.

Highlights

- MRI can detect degeneration due to APP overexpression in mouse olfactory neurons.
- MRI detects recovery of the olfactory bulb after discontinuing APP overexpression.
- Layer specific MRI can assess reagents ability to block olfactory neuronal loss.

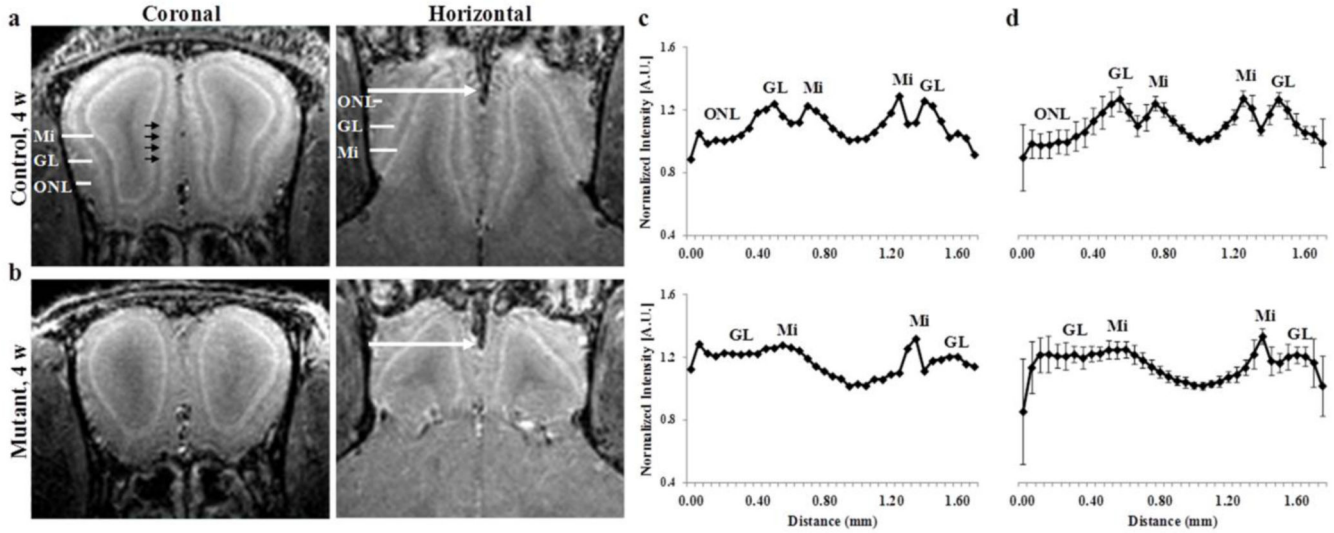

Figure 1.

Coronal and horizontal T_1 weighted images (MEMRI), at 50 μm isotropic resolution, taken 24 h after iv infusion of 100 mM $MnCl_2$ solution of 4 week old (**a**) control and (**b**) mutant mice, and the corresponding normalized (**c**) individual intensity profile and (**d**) group intensity profile. The different layers in the OB are clearly detected in control mouse (**a**) as well as individual glomeruli (shown by the black arrows). The intensity profile was taken for each OB from lateral to medial side across the OB as shown by the white arrows, and normalized to the minimum intensity for each OB. Group intensity profile is the average and sd, of both left and right OB of 3 to 4 week old control (n=4, total of 8 OBs) and mutant (n=4, 8 OBs). ONL – olfactory nerve layer, GL – glomerular layer, Mi – mitral cell layer.

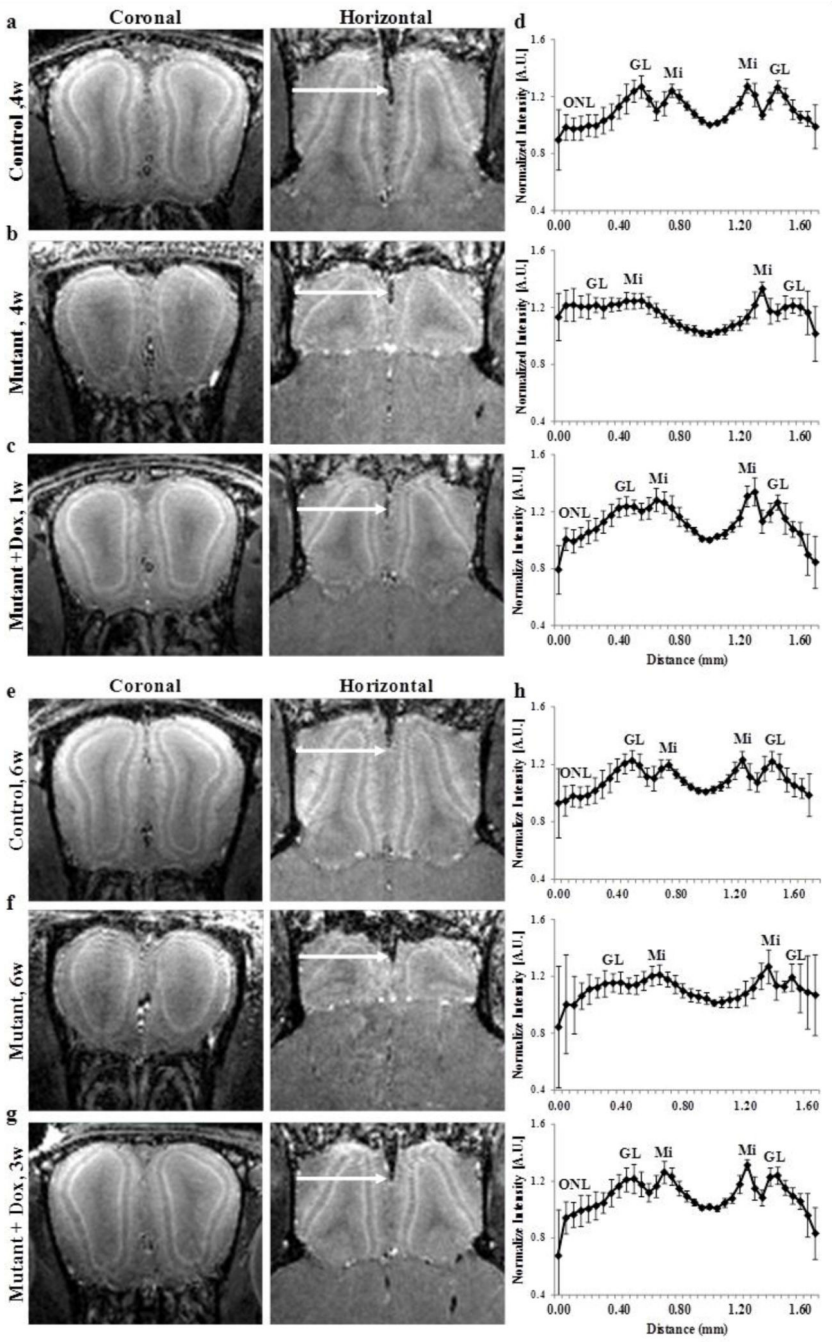

Figure 2.

Coronal and horizontal T_1 weighted images (MEMRI), at 50 μm isotropic resolution, taken 24 h after iv infusion of 100 mM $MnCl_2$ solution of 4 week old (**a**) control, (**b**) mutant and (**c**) mutant mouse after 1 week of doxycycline treatment mice and (**d**) the corresponding group intensity profile of 3 to 4 week old mice groups, and of 8 weeks old **(e)** control (**f**) mutant and (**g**) 7 week old mutant mouse after 3 weeks of doxycycline treatment and (**h**) the corresponding group intensity profile of 6 to 8 week old mice groups. The intensity profile was taken for each OB from lateral to medial side across the OB as shown by the arrows,

and normalized to the minimum intensity for each OB. Group intensity profile is the average and sd, for both left and right OB of 3 to 4 week old control (n=4, total of 8 OBs), mutant (n=4, 8 OBs) and mutant mouse after 1 week of doxycycline treatment (n=4, 8 OBs) and 6 to 8 week old control (n=8, total of 16 OBs), mutant (n=4, 8 OBs), and mutant mouse after 3 weeks of doxycycline treatment (n=5, 10 OBs). ONL – olfactory nerve layer, GL – glomerular layer, Mi – mitral cell layer.

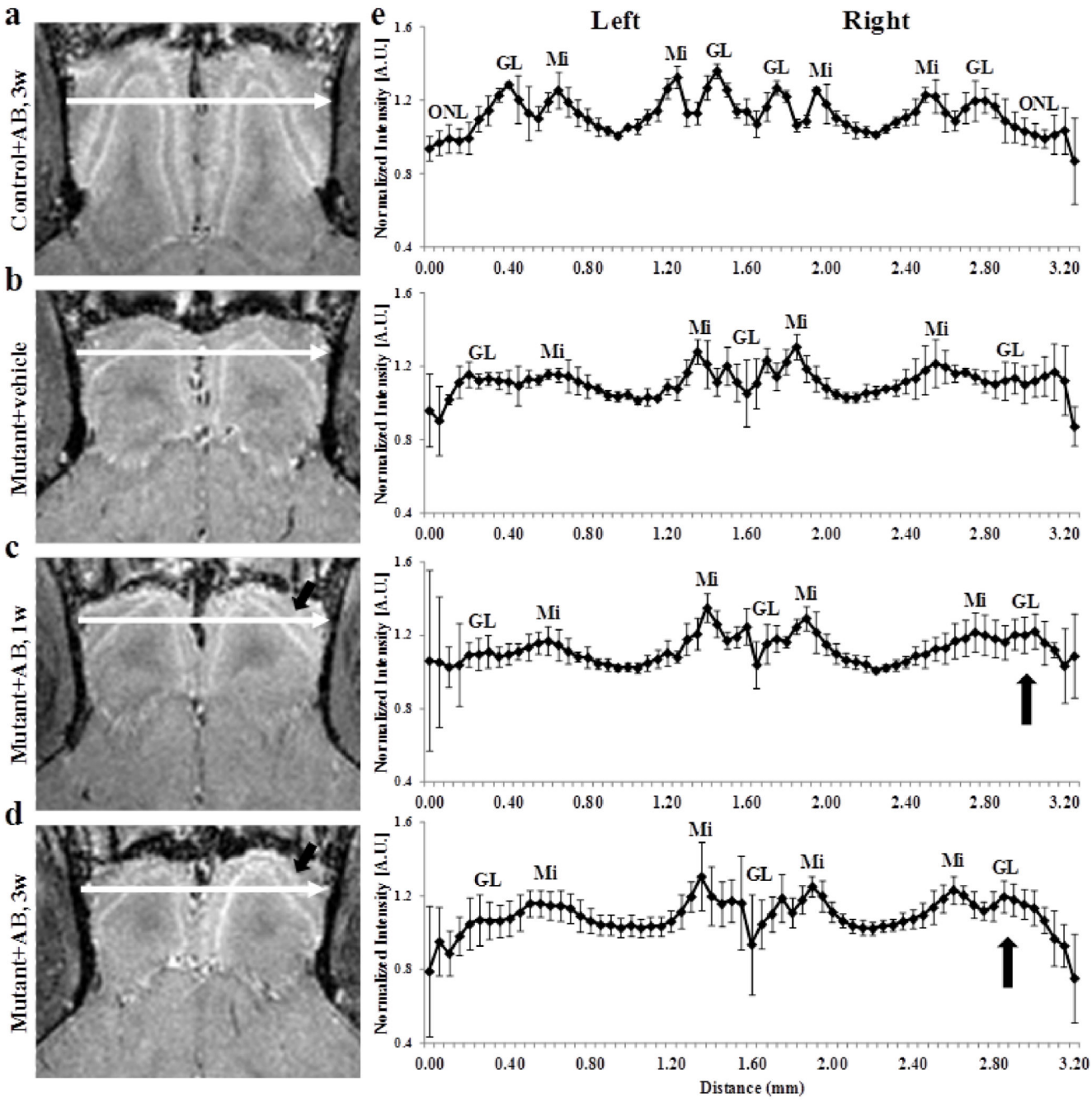

Figure 3.

horizontal T_1 weighted images (MEMRI), at 50 μm isotropic resolution, taken 24 h after iv infusion of 100 mM $MnCl_2$ solution of 7 week old control (**a**) 6 to 8 week old mutant mice after (**b**) 3 weeks of vehicle administration (**c**) 1 week of hAPP antibody administration and (**d**) 3 weeks after antibody administration to the right naris, and (**e**) the corresponding group intensity profiles. The intensity profile was taken across each OB from lateral side of the left OB to the right OB as shown by the arrows, and normalized to the minimum intensity for each OB. Group intensity profiles are the average and sd, for both left and right OB of 6 to 8

week old control after 3 weeks of antibody administration (n=3) and mutant after 3 weeks of vehicle administration (n=4), 1 week of hAPP antibody administration (n=5) and 3 weeks after antibody administration (n=7) to the right naris. ONL – olfactory nerve layer, GL – glomerular layer, Mi – mitral cell layer.

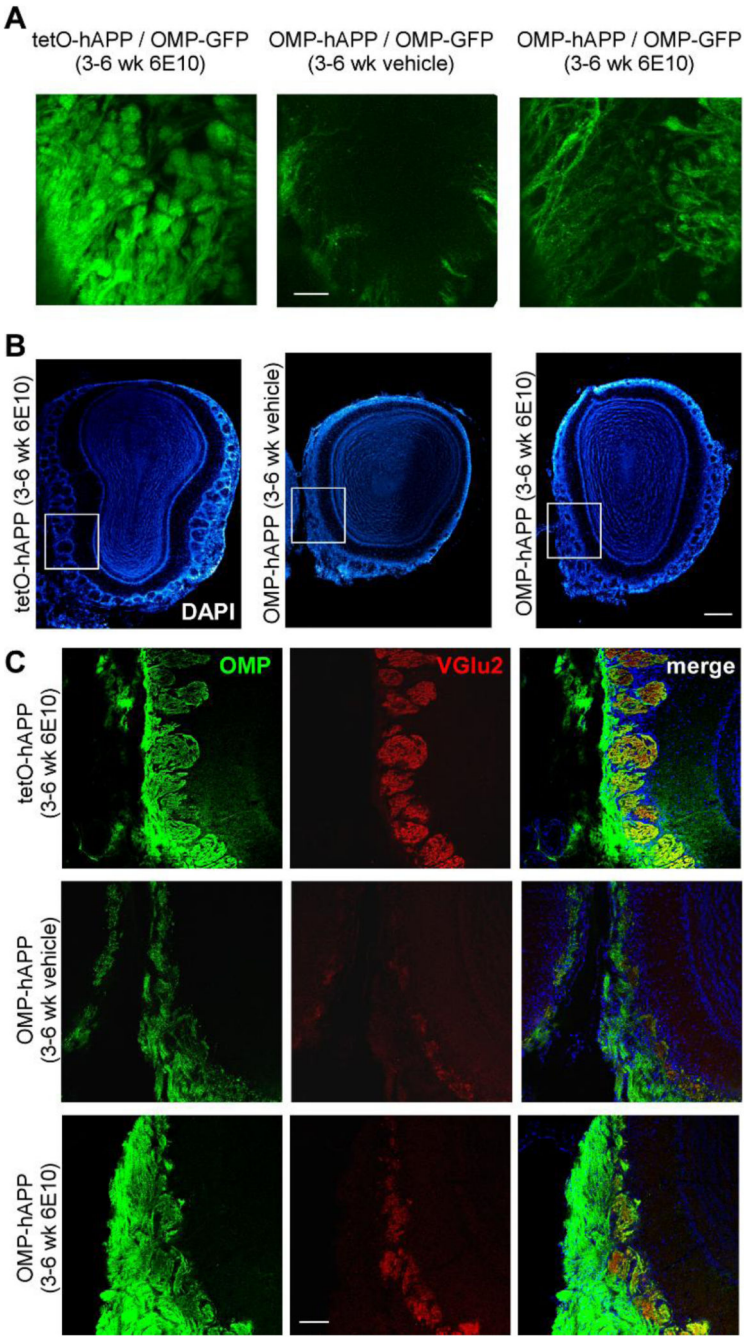

Figure 4.

(**a**) Whole-mount fluorescence imaging of OSNs axons and glomeruli in the OB from 6 week old control after 3 weeks of hAPP antibody (6E10) administration (left) and 6 week old mutant mice after 3 weeks of vehicle administration (middle) and hAPP antibody administration (right) to the right naris. (**b**) Low magnification images of DAPI nuclear staining for the 3 groups of animals (**c**) higher magnification images of OB sections from the 3 groups of animals at 6 week of age: control after 3 weeks of hAPP antibody administration (top row) and mutant after 3 weeks of vehicle administration (middle row) and hAPP

antibody administration (bottom row). First column, OMP immunohistochemistry signal, marking mature OSNs; second column, VGlu2 immunohistochemistry signal, marking synaptic terminal of OSNs; last column, merge of the previous two channels. Scale bar – 4a, 200 μm; 4b low magnitude, 400 μm; 4c high magnitude, 100 μm.

Table 1

OB volume, manganese enhancement of the different layers and the distance between the lateral and medial side of Mi in 3 to 4 week old control and mutant groups.

		Control	Mutant
OB volume (mm^3)		19.8 ± 1.1	11.1 ± 0.9***
Mi to Mi Distance (mm)		0.42 ± 0.03	0.70 ± 0.06***
Layer to minimum ratio	GL	1.17 ± 0.05	1.03 ± 0.05***
	Mi	1.16 ± 0.06	1.09 ± 0.07*

GL – glomerular layer, Mi – mitral cell layer.

* $p < 0.05$

** $p < 0.01$

*** $p < 0.001$.

Table 2

OB volume, manganese enhancement of the different layers and the distance between the lateral and medial side of Mi in 3 to 4 week old and 6 to 8 week old mice groups.

		Control 3-4w	Mutant 3-4w	Mutant + Dox 1w
OB volume (mm^3)		19.8 ± 1.1	11.1 ± 0.9***	11.3 ± 0.5***
Mi to Mi Distance (mm)		0.42 ± 0.03	0.70 ± 0.06***	0.49 ± 0.04$^{**\#\#\#}$
Layer to minimum ratio	GL	1.17 ± 0.05	1.03 ± 0.05***	1.07 ± 0.08***
	Mi	1.16 ± 0.06	1.10 ± 0.07*	1.12 ± 0.09

		Control 6-8w	Mutant 6-8w	Mutant + Dox 3w
OB volume (mm^3)		21.6 ± 1.5	9.1 ± 1.3***	14.1 ± 1.5$^{***\#\#}$
Mi to Mi Distance (mm)		0.44 ± 0.06	0.65 ± 0.03***	0.45 ± 0.03$^{\#\#\#}$
layer to minimum ratio	GL	1.13 ± 0.10	1.03 ± 0.07***	1.12 ± 0.08$^{\#\#}$
	Mi	1.12 ± 0.10	1.10 ± 0.07	1.17 ± 0.08$^{*\#\#}$

Mutant and mutant with Dox vs. control:

Mutant with Dox vs. mutant:

GL – glomerular layer, Mi – mitral cell layer.

* $p < 0.05$

** $p < 0.01$

*** $p < 0.001$.

$^{\#}$ $p < 0.05$

$^{\#\#}$ $p < 0.01$

$^{\#\#\#}$ $p < 0.001$.

Table 3

OB volume, manganese enhancement of the different layers and the distance between the lateral and medial side of Mi of left and right OB in hAPP antibody treated mice groups.

		Control + antibody	Mutant + Vehicle	Mutant + antibody 1w	Mutant + antibody 3w
Left OB					
OB volume (mm^3)		10.3 ± 0.2	3.7 ± 0.5***	4.0 ± 0.7***	3.9 ± 0.4***
Mi to Mi Distance (mm)		0.54 ± 0.05	0.67 ± 0.06*	0.73 ± 0.07**	0.69 ± 0.08*
Layer to minimum ratio	GL	1.19 ± 0.05	1.06 ± 0.07**	1.04 ± 0.06***	1.01 ± 0.06***
	Mi	1.16 ± 0.03	1.11 ± 0.10	1.11 ± 0.06	1.11 ± 0.07
Right OB					
OB volume (mm^3)		10.3 ± 0.3	3.8± 0.4***	4.0 ± 0.6***	3.9 ± 0.5***
Mi to Mi Distance (mm)		0.51 ± 0.03	0.69 ± 0.07***	0.71 ± 0.08*	0.68 ± 0.05**
Layer to minimum ratio	GL	1.15 ± 0.05	1.06 ± 0.05**	1.03 ± 0.02**	1.07 ± 0.06*
	Mi	1.16 ± 0.05	1.12 ± 0.08	1.09 ± 0.07*	1.12 ± 0.07

Mutant treated with vehicle or hAPP antibody vs. control for left and right OB:

GL – glomerular layer, Mi – mitral cell layer.

* $p < 0.05$

** $p < 0.01$

*** $p < 0.001$